XLI CILAMCE
XLI Ibero-Latin American Congress on Computational Methods in Engineering
16-19 November, 2020 FOZ DO IGUAÇU PARANÁ – BRAZIL

Modeling and numerical simulation of crack propagation using peridynamics

Adair R. Aguiar[1], Túlio V. B. Patriota[1],

[1]*Dept. of Structures - SET, University of São Paulo*
Av. Trab. São Carlense, 400 - Parque Arnold Schimidt, São Carlos, 13566-590, São Paulo, Brazil
aguiarar@sc.usp.br, tuliopatriota96@gmail.com

Abstract. Different damage models in peridynamics have been proposed to predict dynamic fracture of brittle materials. The prototype micro-brittle (PMB) material and its modified version, the DTT model, concern a bond-based constitutive model together with bond-breakage damage criteria. These models consider only the elongation of peridynamic bonds with fixed Poisson's ratio. To circumvent this limitation, the state-based model LSJ was recently proposed, which incorporates a dilatation term in its constitutive relations. It concerns an interaction-breakage damage criterion that has two distinct damage factors, one associated with elongation and the other one with dilatation. We modify the LSJ model to obtain bond-breakage damage criteria, called the LSJ-T model. In addition, we also introduce bond-breakage criteria in a two-dimensional ordinary, state-based peridynamic model, which we call the LPS-T model. To compare the crack propagation paths obtained numerically from these damage models, we consider a thin glass plate with an initial semi-crack under mode I loading. Overall, the models were able to grasp the main characteristics of crack propagation, such as crack propagation speed, branching, and crack pattern. The modified version LSJ-T and DTT were the only ones presenting symmetry and no arrested branches in the crack paths, indicating a numerically stable crack propagation.

Keywords: Peridynamics, numerical methods, damage, brittle fracture

1 Introduction

The peridynamic theory is an extension of the classical continuum mechanics theory and is characterized by the integration of the interaction forces between near particles separated by finite distances. These forces depend upon the relative displacements and positions between material points within a body, rather than the spatial derivatives of displacements that are used in classical constitutive relations. Since spatial derivatives are not used, the peridynamic governing equations are valid everywhere in the body, including crack tips and corners.

This new theory was proposed by Silling [1], and it allows for the possibility of considering non smooth functions as candidates for solutions of non smooth problems, such as fracture mechanics problems, where the displacement fields may not even be continuous across crack surfaces. Silling & Askari [2] use a mesh-free numerical method to implement the prototype micro-brittle material (PMB), which is a bond-breakage damage model that yields a good approximation for the fracture energy release rate of classical fracture mechanics. In this model, force and damage functions are discontinuous, which have caused some mathematical difficulties. To obtain a well-posed peridynamic problem, Du et al. [3] propose a modified version, here called the DTT model, which considers that force and damage functions are continuous and piecewise linear functions. Even though these models were able to grasp important features of brittle fracture, they are bond-based peridynamic models, which means that they only consider the strain state of a bond to compose its response, which, in turn, leads to a fixed value for the Poisson's ratio.

A more general theory that takes into account both the dilatational and deviatoric parts of the peridynamic strain state field was proposed by Silling et al. [4] and is called the state-based peridynamic theory. In particular, they introduce the linear peridynamic solid material (LPS) model, which contains material constants that do not require the Poisson's ratio to be fixed. Silling & Askari [5] use the LPS model to formulate a damage model to study fatigue failure in peridynamics. They add bond-breakage damage by bringing to zero the force in a bond when a damage criterion is met. Later, Lipton et al. [6] introduce a damage model, here called the LSJ model, for an isotropic linearly elastic material that depends on two unrelated damage criteria and yields a well-posed

peridynamic problem. Their bond force is zero only when both the damage criteria are met. However, it's not yet clear how one of their damage criteria, which is related to the hydrostatic strain, is connected to physic principles behind fracture dynamics. Further, since this latter criterion is unrelated to the other damage criterion, which considers the bond elongation, a broken bond in terms of elongation may still present reminiscent forces, and thus bond-breakage conditions, which require a zero force in broken bonds, are not met.

The main focus of this work is the modeling of dynamic fracture of solids made of brittle materials using state-based damage models. We introduce modifications into the 2D version for the LPS, obtained by Le et al. [7], and for the LSJ from Lipton et al. [6], which we call the LPS-T and the LSJ-T models, respectively, and use these models together with the PMB and DTT models to simulate crack propagation in a thin glass plate under mode I crack opening. The LSJ-T model modifies the original LSJ model by considering bond-breakage damage, which suits better brittle fracture, rather than interaction-breakage. In the same way, the LPS-T model modifies the original damage-free 2D LPS model in Le et al. [7] to consider bond-breakage. It can be seen as the state-based counterpart of the DTT model.

The other sections of this work are briefly discussed below. In Sec. 2 we provide a theoretical background on modeling of damage using peridynamics. In Sec. 3 we present details of the numerical implementation of the damage models, the results of the numerical simulation of the mode I crack opening of a thin glass plate, and a discussion of these results against well known results from the literature. Lastly, in Sec. 4, we recap the main results of this work and give concluding remarks regarding the advantages and disadvantages of the modified state-based models in simulating brittle fracture against their bond-based counterparts.

2 Theoretical background

Let $\mathcal{B} \subset \mathbb{E}^2$ be the reference configuration of a solid body at time $t = 0$ and $\boldsymbol{\chi}(\mathbf{x}, t)$ be the position of point $\mathbf{x}$ at time t, with $\mathbb{E}^2$ being the two-dimensional Euclidean space. Let also $\mathcal{N}_\delta$ be a δ-neighborhood of $\mathbf{x}$, where, in peridynamics, the radius δ is called the horizon. Here, $\mathcal{N}_\delta$ is a circle of radius δ centered at $\mathbf{x}$. The relative position vector $\boldsymbol{\xi} = \mathbf{x}' - \mathbf{x}$ is called a bond and the set of all bonds is denoted by $\mathcal{H}_\delta$.

A peridynamic state is a tensorial function of the form $\underline{\mathbf{A}}(\mathbf{x}, t)\,\langle\cdot\rangle : \mathcal{H}_\delta \to \mathcal{L}_m$, where $\mathcal{L}_m$ is the set of m-th order tensors; if $m = 1$, the state is a vector and, if $m = 0$, a scalar. In peridynamics, deformation measures are defined in terms of difference displacement fields, which are defined through $\underline{\mathbf{u}}\,\langle\boldsymbol{\xi}\rangle \equiv \boldsymbol{\eta} = \mathbf{u}(\mathbf{x} + \boldsymbol{\xi}) - \mathbf{u}(\mathbf{x})$.Thus, the strain state (sometimes called the relative elongation state) of a bond $\boldsymbol{\xi}$ at $\mathbf{x}$, is the counterpart of the normal strain from classical continuum mechanics and is defined through

$$\underline{s}\,\langle\boldsymbol{\xi}\rangle = \frac{\underline{e}\,\langle\boldsymbol{\xi}\rangle}{|\boldsymbol{\xi}|}, \qquad \underline{e}\,\langle\boldsymbol{\xi}\rangle \equiv |\boldsymbol{\eta} + \boldsymbol{\xi}| - |\boldsymbol{\xi}|\,. \tag{1}$$

We can obtain the infinitesimal normal strain state by linearizing eq. (1), thus obtaining

$$\underline{\epsilon}\,\langle\boldsymbol{\xi}\rangle = \frac{\boldsymbol{\xi}\cdot\boldsymbol{\eta}}{|\boldsymbol{\xi}|^2}. \tag{2}$$

The peridynamic equation of motion is given by

$$\rho\,\ddot{\mathbf{u}}(\mathbf{x}, t) = \int_{\mathcal{N}_\delta} \mathbf{f}(\mathbf{x}, \mathbf{x}', \underline{\mathbf{u}}, t)\,dV_{\mathbf{x}'} + \mathbf{b}(\mathbf{x}, t), \tag{3}$$

where $\ddot{\mathbf{u}}(\mathbf{x}, t)$ is the acceleration of point $\mathbf{x} \in \mathcal{B}$ at time t, ρ is the mass density, $\mathbf{f}$ is the interaction force function in the peridynamic bond between the points $\mathbf{x}$ and $\mathbf{x}'$, and $\mathbf{b}$ is the body force density. We may interpret the integral term as the sum of the contribution forces that all the points within the δ-neighborhood of point $\mathbf{x}$ exert on $\mathbf{x}$ itself. Here, the unit of the interaction force $\mathbf{f}$ is force per volume squared.

In this work, we consider isotropic elastic materials. The PMB material model, proposed by Silling & Askari [2], is a suitable constitutive relation between the interaction force $\mathbf{f}$ and the difference displacement field $\underline{\mathbf{u}}$, which is given by

$$\mathbf{f}(\mathbf{x}, \mathbf{x}', \underline{\mathbf{u}}) \equiv \hat{\mathbf{f}}(\boldsymbol{\xi}, \boldsymbol{\eta}) = \underline{f}\,\langle\boldsymbol{\xi}\rangle\,\underline{\mathbf{e}}\,\langle\boldsymbol{\xi} + \boldsymbol{\eta}\rangle\,, \qquad \underline{f}\,\langle\boldsymbol{\xi}\rangle = \mu(\underline{s}^*\,\langle\boldsymbol{\xi}\rangle)\,\underline{c}\,\langle\boldsymbol{\xi}\rangle\;\underline{s}\,\langle\boldsymbol{\xi}\rangle \tag{4}$$

where $\hat{\mathbf{f}}$ is the pairwise force function, $\underline{\mathbf{e}}\,\langle\boldsymbol{\xi} + \boldsymbol{\eta}\rangle$ is the unitary vector in the direction of the deformed bond $\boldsymbol{\xi} + \boldsymbol{\eta}$, $\underline{f}$ is the pairwise force scalar state, the scalar state $\underline{c}\,\langle\boldsymbol{\xi}\rangle$ is the micro-modulus function, $\mu : \mathbb{R} \to [0, 1]$ is the damage factor function and $\underline{s}^*$ is the maximum relative elongation the bond underwent until the evaluation time, i.e.

$$\mu(\underline{s}^*) = \begin{cases} 1, & \underline{s}^* < S_c, \\ 0, & \underline{s}^* \geq S_c, \end{cases} \qquad \underline{s}^*(\mathbf{x}, t)\,\langle\boldsymbol{\xi}\rangle = \max_{0 \leq l \leq t} \left(\underline{s}\,\langle\boldsymbol{\xi}\rangle\right), \tag{5}$$

where S_c is the critical relative elongation. By using the history of the elongation as argument, the damage factor enforces irreversible breakage of a bond. Thus, once it is broken, it remains broken, having zero force thereafter. The micro-modulus function can be expressed as

$$\underline{c}\,\langle\boldsymbol{\xi}\rangle = C\,\omega(|\boldsymbol{\xi}|)|\boldsymbol{\xi}|, \qquad C = \frac{6\,E}{m}, \tag{6}$$

where $\omega(|\boldsymbol{\xi}|)$ is a generic influence function, E is the Young's modulus, and m is the weighted volume given by

$$m = \int_{\mathcal{H}_\delta} \omega(|\boldsymbol{\zeta}|)|\boldsymbol{\zeta}|^2\, dV_{\boldsymbol{\zeta}}. \tag{7}$$

In this work, we consider $\omega(|\boldsymbol{\xi}|) = \omega_\delta(|\boldsymbol{\xi}|)/|\boldsymbol{\xi}|$ for $|\boldsymbol{\xi}| \leq \delta$ and $\omega(|\boldsymbol{\xi}|) = 0$, otherwise, where ω_δ is the conical influence function, given by

$$\omega_\delta(r) = 1 - \frac{r}{\delta}. \tag{8}$$

Du et al. [3] propose a modified version of the PMB model, here called the DTT model, to formulate a well-posed peridynamic problem. They consider that both the force scalar state and the damage factor are continuous. Instead of eq. (4.b), their modified DTT pairwise force scalar state is

$$\underline{f} = \overline{\mu}(\underline{s}^*)\,\underline{c}\,F(\underline{s}), \tag{9}$$

where the bond dependence is omitted for simplicity, $\underline{c}$ is given by eq. (6),

$$F(x) = \begin{cases} \mathcal{S}_0^- \frac{x-\mathcal{S}_1^-}{\mathcal{S}_0^- - \mathcal{S}_1^-}, & \text{if } x \in (\mathcal{S}_1^-, \mathcal{S}_0^-), \\ x, & \text{if } x \in [\mathcal{S}_0^-, \mathcal{S}_0^+], \\ \mathcal{S}_0^+ \frac{\mathcal{S}_1^+ - x}{\mathcal{S}_1^+ - \mathcal{S}_0^+}, & \text{if } x \in (\mathcal{S}_0^+, \mathcal{S}_1^+), \\ 0, & \text{otherwise}, \end{cases} \qquad \overline{\mu}(x) = \begin{cases} 1, & \text{if } x \in [-1, \mathcal{S}_0^+), \\ \frac{\mathcal{S}_1^+ - x}{\mathcal{S}_1^+ - \mathcal{S}_0^+}, & \text{if } x \in [\mathcal{S}_0^+, \mathcal{S}_1^+), \\ 0, & \text{otherwise}, \end{cases} \tag{10}$$

and

$$\mathcal{S}_0^+ = 0.95 S_c, \qquad \mathcal{S}_1^+ = 1.05 S_c, \qquad \mathcal{S}_0^- = -0.98, \qquad \mathcal{S}_1^- = -0.99. \tag{11}$$

Both the PMB and the DTT models are bond-based models, which implies that the Poisson's ratio ν has a fixed value that is equal to 1/3 for the plane stress conditions considered in this work. For the more complete state-based theory, for which the Poisson's ratio is not fixed, the interaction force function $\mathbf{f}$ that appears in eq. (3) is of the form $\mathbf{f}(\mathbf{x}, \mathbf{x}', \mathbf{u}) = \underline{\mathbf{T}}(\mathbf{x}, \mathbf{u})\,\langle\boldsymbol{\xi}\rangle - \underline{\mathbf{T}}(\mathbf{x}', \mathbf{u})\,\langle -\boldsymbol{\xi}\rangle$,where $\underline{\mathbf{T}}(\mathbf{x}, \mathbf{u})\,\langle\boldsymbol{\xi}\rangle$ and $\underline{\mathbf{T}}(\mathbf{x}', \mathbf{u})\,\langle -\boldsymbol{\xi}\rangle$ are force vector states evaluated on bonds $\boldsymbol{\xi}$ and $-\boldsymbol{\xi}$, respectively, and acting at the points $\boldsymbol{\chi}(\mathbf{x})$ and $\boldsymbol{\chi}(\mathbf{x}')$ in the deformed configuration $\boldsymbol{\chi}(\mathcal{B})$. Ordinary state-based materials have their force vector state acting along the direction of the deformed bond, which can be written in the form

$$\underline{\mathbf{T}}(\mathbf{x}, \underline{\mathbf{u}})\,\langle\boldsymbol{\xi}\rangle = \underline{t}\,\langle\boldsymbol{\xi}\rangle\ \underline{\mathbf{e}}\,\langle\boldsymbol{\xi} + \boldsymbol{\eta}\rangle\,, \tag{12}$$

where $\underline{t}$ is the force scalar state. A state-based model commonly used in peridynamics is the LPS model proposed by Silling et al. [4]. It contains both dilatational and deviatoric parts of the peridynamic deformation state in its constitutive response. For plane stress conditions, Le et al. [7] show that the force scalar state $\underline{t}$ in (12) is given by

$$\underline{t}\,\langle\boldsymbol{\xi}\rangle \;=\; \frac{2\,(2\,\nu - 1)}{\nu - 1}\left(\hat{c}_1\theta - \frac{\hat{c}_2}{3}\int_{\mathcal{H}_\delta} \omega(|\boldsymbol{\zeta}|)\underline{e}^d\,\langle\boldsymbol{\zeta}\rangle\,|\boldsymbol{\zeta}|\; dV_{\boldsymbol{\zeta}}\right)\frac{\omega(|\boldsymbol{\xi}|)\,|\boldsymbol{\xi}|}{m} + \hat{c}_2\,\omega(|\boldsymbol{\xi}|)\,\underline{e}^d\,\langle\boldsymbol{\xi}\rangle\,, \tag{13}$$

where $\hat{c}_1 = E/\left[3(1-2\nu)\right] + E/\left[18(1+\nu)\right]\,(\nu+1)^2/(2\nu-1)^2$, $\hat{c}_2 = 8\,E/[2\,m\,(\nu+1)]$, with m being the weighted volume given by eq. (7), $\underline{e}^d = \underline{e} - \frac{\theta\,m}{3}$ is the deviatoric part of the elongation state $\underline{e}$, and

$$\theta(\mathbf{x}, \underline{\mathbf{u}}) = \frac{2(2\nu-1)}{\nu-1}\frac{1}{m}\int_{\mathcal{H}_\delta} \omega(|\boldsymbol{\zeta}|)\,|\boldsymbol{\zeta}|\,\underline{e}\,\langle\boldsymbol{\zeta}\rangle\; dV_{\boldsymbol{\zeta}} \tag{14}$$

is the dilatational part of $\underline{e}$, which can be seen as the peridynamic counterpart of the hydrostatic strain in classical linear elasticity. In this work we modify the force scalar state in eq. (13) to introduce bond-breakage damage as

$$\underline{t}_{\text{LPS-T}}\,\langle\boldsymbol{\xi}\rangle = \left[\frac{c_1}{m}\,\theta_{\text{dam}} + c_2\,F(\underline{s})\right]\overline{\mu}(\underline{s}^*)\omega(|\boldsymbol{\xi}|)\,|\boldsymbol{\xi}|\,, \tag{15}$$

where $c_1 = E\,(1-3\,\nu)/[(\nu+1)\,(2\nu-1)]$, $c_2 = \hat{c}_2 = 8\,E/[2\,m\,(\nu+1)]$, and

$$\theta_{\text{dam}}(\mathbf{x},\underline{\mathbf{u}}) = \frac{2(2\nu-1)}{\nu-1}\frac{1}{m}\int_{\mathcal{H}_\delta}\omega(|\boldsymbol{\zeta}|)\,|\boldsymbol{\zeta}|^2\,\underline{s}\,\overline{\mu}(\underline{s}^*)dV_{\boldsymbol{\zeta}} \tag{16}$$

is the dilatation including damage and $\underline{s}$ is the elongation state introduced in eq. (1). Thus, we consider the concept of bond-breakage damage used in Silling & Askari [5], by requiring that the force vector state $\underline{\mathbf{T}}\,\langle\boldsymbol{\xi}\rangle$ be null if the bond $\boldsymbol{\xi}$ is broken since, for $\overline{\mu}(\underline{s}^*)=0$, $\underline{t}_{\text{LPS-T}}\,\langle\boldsymbol{\xi}\rangle = 0$ in eq. (15). We refer to this model as the LPS-T model.

Another model used in this work is derived from the linearized state-based damage model proposed by Lipton et al. [6], here called the LSJ model. This model has two unrelated damage factors: one of them depends on the bond elongation while the other one depends on the dilatation on the points connected by the bond. The model presents interaction-breakage damage conditions, which here means that the breakage of bond requires the failure of not only the bond itself, but of a collection of bonds around it. In order to enforce bond-breakage damage, which suits brittle fracture, we modify the LSJ model to propose a linearized constitutive relation for the force vector state in eq. (12), which is given by

$$\underline{\mathbf{T}}_{\text{LSJ-T}}\,\langle\boldsymbol{\xi}\rangle = \underline{t}_{\text{LST-T}}\,\langle\boldsymbol{\xi}\rangle\;\underline{\mathbf{e}}\,\langle\boldsymbol{\xi}\rangle\,, \tag{17}$$

$$\underline{t}_{\text{LSJ-T}}\,\langle\boldsymbol{\xi}\rangle = \left[\frac{c_1}{m}\tilde{\mu}(\underline{\epsilon}\,\langle\boldsymbol{\xi}\rangle)\,\tilde{\theta}_{\text{dam}} + c_2\,\underline{\epsilon}\,\langle\boldsymbol{\xi}\rangle\right]\tilde{\mu}(\underline{\epsilon}\,\langle\boldsymbol{\xi}\rangle)\,\omega(|\boldsymbol{\xi}|)\,|\boldsymbol{\xi}|\,, \tag{18}$$

where

$$\tilde{\theta}_{\text{dam}} = \frac{2(2\nu-1)}{\nu-1}\frac{1}{m}\int_{\mathcal{H}_\delta}\omega(|\boldsymbol{\xi}|)\,|\boldsymbol{\xi}|^2\,\underline{\epsilon}\,\tilde{\mu}(\underline{\epsilon})dV_{\boldsymbol{\xi}}, \qquad \tilde{\mu}(\underline{\epsilon}) = h\left(\int_0^t j_s(\underline{\epsilon}\,\langle\boldsymbol{\xi}\rangle)d\tau\right) \tag{19}$$

are the linearized dilatation and the model's damage function, respectively. In eq. (19.b), we have that

$$h(x) = \begin{cases} \exp\left[1-\frac{1}{1-(x/x_c)^{2.01}}\right], & \forall x\in(0,x_c),\\ 1, & \forall x\le 0,\\ 0, & \forall x\ge x_c,\end{cases} \qquad j_s(x) = \begin{cases} \frac{(x/S_c-1)^5}{1+(x/S_c)^5}, & \forall x\in[S_c,\infty]\,,\\ 0, & \text{otherwise},\end{cases} \tag{20}$$

where, here, $x_c = j_s(1.05\,S_c)\,\delta t$, with δt being the time increment in the numerical simulation. We refer to this model as the LSJ-T model. It is worth mentioning that, whilst the LSJ model proposed by Lipton et al. [6] has two unrelated damage factors, one for failure due to bond stretch and the other one for failure due to dilatation, the latter is not dominant in bond-breakage conditions and, for this reason, is not introduced in the constitutive relations of the LSJ-T model above. It is also worth noticing that the main differences between the LSJ-T and the LPS-T models lie on the definition of their damage factors and on the linearity of the constitutive relations of the LSJ-T model, inherited from the LSJ model.

In order to find the critical relative elongation state S_c, let us consider a homogeneous body subjected to isotropic extension ($\boldsymbol{\eta} = s\,\boldsymbol{\xi}$). Bonds that cross a fracture surface cannot sustain any forces and are, therefore, broken. The energy per unit fracture length for complete separation of the two halves of the body is called the fracture energy. In 2D, Ha & Bobaru [8] evaluate the fracture energy G_0 as the energy required to break all bonds as the crack advances a unit length. For a PMB bond-based model, this fracture energy is given by

$$G_0 = 2\int_0^\delta\int_z^\delta\int_0^{\arccos(z/\xi)} C\,\omega(\xi)\,\xi^2\,\frac{S_c^2}{2}\,\xi\,d\phi\,d\xi\,dz, \tag{21}$$

where $\xi = |\boldsymbol{\xi}|$. Using eq. (21) together with the conical influence function given by eq. (8), it can be shown that

$$S_c = \sqrt{\frac{5\,\pi\,G_0}{9\,E\,\delta}}. \tag{22}$$

For the state-based models, we propose to find the critical relative elongation by using a similar argument as for the PMB, which consists of equating the strain energy expended by a crack advancing a unit length with the fracture energy G_0 through

$$\begin{aligned} G_0 &= 2\int_0^\delta\left\{\int_z^\delta\int_0^{\arccos z/\xi} c_2\,\omega(\xi)\,\xi^2\,S_c^2\,\xi\,d\phi\,d\xi + c_1\left[\frac{2(2\nu-1)}{\nu-1}\frac{1}{m}\int_z^\delta\int_0^{\arccos z/\xi}\omega(\xi)\,\xi^2\,S_c\,\xi\,d\phi\,d\xi\right]^2\right\}dz\\ &= [c_1\,I_1 + c_2\,I_2]\,S_c^2\,, \end{aligned} \tag{23}$$

where I_1 and I_2 correspond to the integrals multiplying the material constants c_1 and c_2, respectively. If $\nu = 1/3$, $c_1 = 0$ and eq. (23) reduces to eq. (21). For Poisson's ratios different from 1/3, we have an extra-term $c_1\, I_1$ that accounts for the energy lost by the dilatational term. The evaluation of I_1 is complex and requires numerical integration techniques. It can be shown, however, that, for $\nu \in (0, 0.5)$, $c_2 I_2 >> c_1 I_1$. Therefore, we can derive an expression for S_c considering only $c_2\, I_2$, yielding, for a conical influence function,

$$S_c = \sqrt{\frac{5\,(1+\nu)\,\pi\,G_0}{12\,E\,\delta}}. \tag{24}$$

3 Numerical implementation and results

In general, exact solutions of peridynamic problems are not known. To advance our understanding on the subject and to obtain results of practical interest, it is necessary to find approximate solutions of these problems by using a numerical method that is usually based on a quadrature scheme for the integrals together with a finite difference technique for the differentiation in time of the displacement field.

To approximate the two-dimensional domain $\mathcal{B}$ introduced in Section 2, we consider a homogeneous grid, denoted by $\mathcal{B}_D$, of spacing h in both x and y directions. More specifically, $\mathcal{B}_D$ is the union of subdomains τ_i with areas h^2, densities ρ_i, and centroid positions $\mathbf{x}_i \in \mathcal{B}$. Thus, the area of $\mathcal{B}_D$ is the sum of the areas of the subdomains and approximates the area of $\mathcal{B}$, being equal to the area of $\mathcal{B}$ in the case of rectangular domains.

To discretize in time, let us define $t_n = t_{n-1} + \Delta t$, $n = 1, 2, \ldots$, in which the initial time t_0 is usually zero and Δt is a time increment discussed below. The governing equation given by eq. (3) is spatially integrated using a mid-point quadrature rule. Thus, at a point $\mathbf{x}_i \in \mathcal{B}_D$, the discrete governing equation can be written as

$$\rho_i \ddot{\mathbf{u}}_i^n = \sum_{j \in \mathcal{F}_i} \mathbf{f}_{ij}^n \Delta V_{ij} + \mathbf{b}_i^n, \tag{25}$$

where $\ddot{\mathbf{u}}_i^n = \ddot{\mathbf{u}}(\mathbf{x}_i, t_n)$, $\mathbf{b}_i^n = \mathbf{b}(\mathbf{x}_i, t_n)$, $\mathcal{F}_i$ is a set of indices of quadrature points contained in the δ-neighborhood of the ith-node, $\mathbf{f}_{ij}^n = \mathbf{f}(\mathbf{x}_i, \mathbf{x}_j, \underline{\mathbf{u}}, t_n)$ is the interaction force between nodes with indices i and $j \in \mathcal{F}_i$, and ΔV_{ij} is the partial area of the cell τ_j within the δ-neighborhood of the i-th node. For the evaluation of partial areas and of the set $\mathcal{F}_j$, we use an analytical method described in Seleson [9]. For the time integration of eq. (25), we use the velocity Verlet scheme described in Parks & Plimpton [10]. Since this scheme is explicit, the time increment $\Delta\, t$ has to be small enough to ensure stability. In view of this, we use an adapted version of the maximum allowable time increment proposed by Silling & Askari [2]. The simulations were run in MATLAB and the source code can be found at `https://github.com/TulioVBP/PDLAB`.

To compare the different damage models introduced in Section 2, we have considered the propagation of an initial crack in a plate under mode I loading, as depicted in Fig. 1, where we have considered the sudden application of the traction load $\sigma = 4\,\mathrm{MPa}$. To be consistent with the peridynamic theory, this load is converted into an equivalent body force acting on nodes of the domain $\mathcal{B}_D$ that are within a distance from both the top and the bottom edges. In this work, this distance is δ. The crack propagation is measured by the damage index $\phi(x)$, defined by

$$\phi(\mathbf{x}) = 1 - \frac{\int_{\mathcal{H}_\delta} \underline{H}\,\langle \boldsymbol{\xi} \rangle \; dV_{\boldsymbol{\xi}}}{\int_{\mathcal{H}_\delta} \; dV_{\boldsymbol{\xi}}}, \qquad \mathbf{x} \in \mathcal{B}\,, \tag{26}$$

where $\underline{H}\,\langle \boldsymbol{\xi} \rangle$ is the damage factor of a damage model considered in this work, which is given by eq. (5.a) for the PMB model, eq. (10.b) for both the DTT and LPS-T models, and eq. (19.b) for the LSJ-T model. Thus, $\phi(\mathbf{x})$ multiplied by 100 yields the percentage of broken bonds of point $\mathbf{x}$. Points on the surface of a straight crack, theoretically, have half of their bonds broken since they only terminate interactions with the half of the body across the crack. If the crack isn't straight, this index can reach values higher or slightly lower than 0.5.

The plate is made of soda-lime glass, with Young's modulus $E = 72\,\mathrm{GPa}$, Poisson's ratio $\nu = 0.22$, density $\rho = 2440\,\mathrm{kg\,m^{-3}}$, and fracture energy $G_0 = 3.8\,\mathrm{J\,m^{-2}}$. In our simulations we consider a horizon $\delta = 1\,\mathrm{mm}$, which is sufficiently small when compared to the dimensions of the plate. For the spatial integration, we consider a mesh ratio $d = h/\delta = 4$, which is a good tradeoff between numerical accuracy and computational cost. For the time integration, we consider the time increment $\Delta t = 0.02\,\mu\mathrm{s}$, with a final time $t_{\text{final}} = 30\,\mu\mathrm{s}$.

In Fig. 2 we show damage color maps for the damage models (a) DTT, (b) LPS-T, (c) PMB, and (d) LSJ-T, where the color vary from red, representing points with damage index greater than 0.5, to dark blue, representing points with damage index close to zero. The captions for each model also contain the angle between the upper crack branch of the first branching event and the horizontal mid line. For points $\mathbf{x}$ at the red regions in Fig. 2,

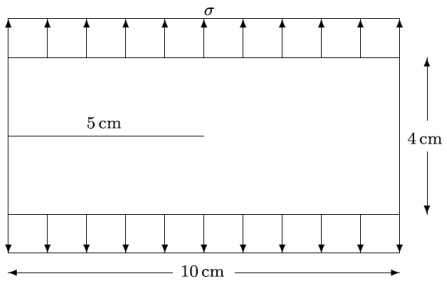

Figure 1. Soda-lime glass under tensile test with a pre-existent crack.

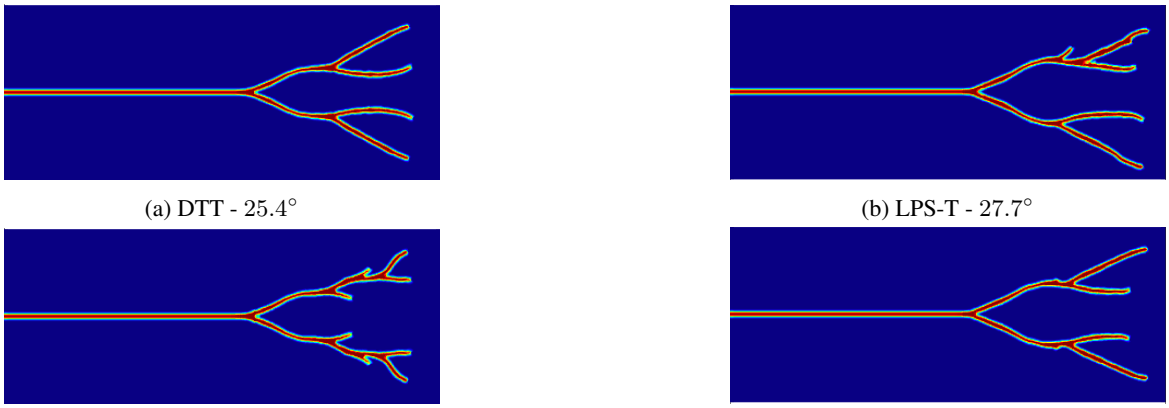

(a) DTT - 25.4°

(b) LPS-T - 27.7°

(c) PMB - 25.4°

(d) LSJ-T - 26.6°

Figure 2. Damage maps of glass plate depicted in Fig. 1 after second crack branching.

$\phi(\mathbf{x}) > 0.5$, which means that the central lines of these red regions correspond to crack paths. For all the models, a crack advances in a straight line before branching into two new branches. As the crack progresses after the first crack branching, the phenomenon of double crack branching is well captured by the numerical crack patterns as they resemble the experimental benchmark presented in Fig. 3 for a mode I loading experiment performed by Bowden et al. [11] in a glass plate with an initial blunt notch. At the first crack branching, the opening angles for the state-based models LPS-T and LSJ-T, given by, respectively, $27.7°$ and $26.6°$, are slightly larger than the angle for both the DTT and the PMB models, given by $25.4°$, since the state-based models have different Poisson's ratio ($\nu = 0.22$) than the bond-based models, in which the Poisson's ratio is constrained to 1/3 (see Silling et al. [12]).

Although formulated as a symmetric problem, the numerical problem of crack propagation is not symmetric because of round-off errors, which may cause crack path asymmetries that are exacerbated by the sensitivity to small perturbations in unstable dynamic crack propagation (see Ha & Bobaru [11], Bobaru & Zhang [12]). Pronounced asymmetry of crack pattern, observed in Fig. 2.(b) for the LPS-T model, and arrested crack branches, observed in Fig. 2.(b) and Fig. 2.(c) for the LPS-T and PMB models, respectively, are features that suggest unstable crack propagation. None of these features are observed in Fig. 2.(a) and in Fig. 2.(d), which suggests that the DTT and LSJ-T models present the most stable crack propagation.

Abraham [13] states that the maximum theoretical speed a crack can propagate is the Rayleigh wave speed, which is the sound wave speed in the material. This happens because, for the crack to be propagated, the necessary energy to break the atomic bonds must be provided at the crack tip, and such energy is traveling in the material at

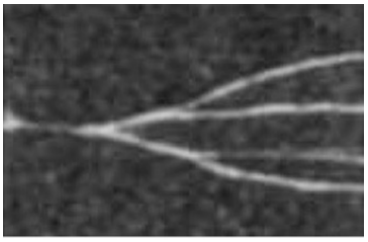

Figure 3. Experimental result obtained by Bowden et al. [11] for a glass plate with blunt pre-notch.

the Rayleigh wave speed. In Fig. 4 we show the propagation speed of the crack tip normalized by the Rayleigh wave speed of soda-lime glass, given by $C_r \approx 3180\,\mathrm{m\,s^{-1}}$, plotted against the simulation time for the different damage models considered in Fig. 2. We also show the constant line corresponding to $2\,C_r/3$. In order to calculate the propagation speed of the cracks, we track the farthest point to the right that has damage index greater than 0.3. We have verified that values in the range $(0.2, 0.4)$ do not change much the results of Fig. 4.

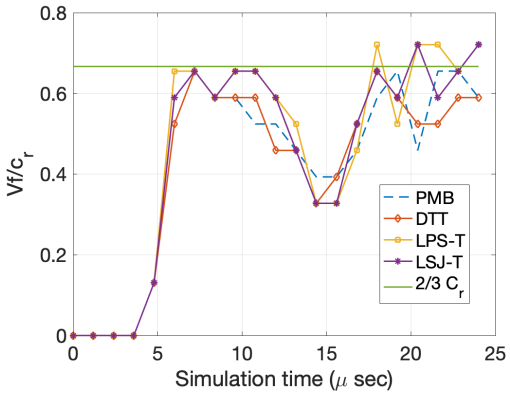

Figure 4. Crack tip propagation speeds for mode I loading on a plate with an initial semi-crack.

Experimental results for an amorphous material have shown that the crack propagation never reaches the Rayleigh limit, losing stability and branching when reaching values of 0.35-0.65 of the Rayleigh wave speed (see Döll [14], Ravi-Chandar & Knauss [15]). By comparing the velocity profiles, we note that they are similar qualitatively. The normalized speed is zero until the time the crack starts propagating at about $4\,\mu$s. Thereafter, the speed rapidly reaches the maximum expected speed and oscillates about this maximum speed until right after the crack branching occurs at about $8\,\mu$s. It then starts decreasing until the time the crack stops branching at about $15\,\mu$s. At this time new cracks start propagating and, again, the speed reaches the maximum speed and oscillates about this speed until the next branching occurs, at about $20\,\mu$s. Ramulu & Kobayashi [16] and Döll [14] have shown that the decrease in the crack tip speed after the crack branching event is also observed experimentally. Note that the maximum crack tip speed is slightly greater than $2/3\,C_r$ for all the models, but still smaller than the Rayleigh wave speed. This high propagation speed can be related to the high traction forces considered. After the second branching, it is not well defined which tip to follow, mainly for results with multiple arrested minor branches; so the crack propagation speed is not interpreted there.

As a final remark, the computational costs of the simulations with the state-based models were, on average, 40% higher than their counterparts with the bond-based models. The additional computational time is due to extra evaluations of dilatational terms in the state-based models.

4 Conclusions

In this work we have introduced two modified versions of state-based damage models found in the literature that are suitable for brittle fracture modeling. We have validated the models with a benchmark experiment of mode I loading and have shown that the new state-based models grasped well the characteristics of brittle fracture, like the crack branching and crack propagation speed. The computational cost is, however, 40% higher than their bond-based counterparts. In addition, the LSJ-T and DTT models are promising, as they seem to be more stable than the other models, especially after the initiation of the second crack branching.

Acknowledgements. Support of São Paulo Research Foundation (FAPESP), grants n° $2019/00428-7$ and n° $2020/04750-8$, is gratefully acknowledged. The first author also acknowledges the support of National Council for Scientific and Technological Development (CNPq), grant n° $420099/2018-2$.

Authorship statement. The authors hereby confirm that they are the sole liable persons responsible for the authorship of this work, and that all material that has been herein included as part of the present paper is either the property (and authorship) of the authors, or has the permission of the owners to be included here.

References

[1] Silling, S. A., 2000. Reformulation of elasticity theory for discontinuities and long-range forces. *Journal of the Mechanics and Physics of Solids*, vol. 48, n. 1, pp. 175–209.
[2] Silling, S. A. & Askari, E., 2005. A meshfree method based on the peridynamic model of solid mechanics. *Computers & structures*, vol. 83, n. 17-18, pp. 1526–1535.
[3] Du, Q., Tao, Y., & Tian, X., 2018. A peridynamic model of fracture mechanics with bond-breaking. *Journal of Elasticity*, vol. 132, n. 2, pp. 197—-218.
[4] Silling, S. A., Epton, M., Weckner, O., Xu, J., & Askari, E., 2007a. Peridynamic States and Constitutive Modeling. *Journal of Elasticity*, vol. 88, n. 2, pp. 151–184.
[5] Silling, S. A. & Askari, A., 2014. Peridynamic model for fatigue cracking. *SAND2014-18590. Albuquerque: Sandia National Laboratories*.
[6] Lipton, R., Said, E., & Jha, P., 2018. Free Damage Propagation with Memory. *Journal of Elasticity*, vol. 133, n. 2, pp. 129–153.
[7] Le, Q. V., Chan, W. K., & Schwartz, J., 2014. A two-dimensional ordinary, state-based peridynamic model for linearly elastic solids. *International Journal for Numerical Methods in Engineering*, vol. 98, n. 8, pp. 547–561.
[8] Ha, Y. D. & Bobaru, F., 2010. Studies of dynamic crack propagation and crack branching with peridynamics. *International Journal of Fracture*, vol. 162, n. 1, pp. 229–244.
[9] Seleson, P., 2014. Improved one-point quadrature algorithms for two-dimensional peridynamic models based on analytical calculations. *Computer Methods in Applied Mechanics and Engineering*, vol. 282, pp. 184–217.
[10] Parks, M. L. & Plimpton, S. J., 2008. PDLAMMPS 0.1. Technical report, Sandia National Laboratories.
[11] Bowden, F. P., Brunton, J. H., Field, J. E., & Heyes, A. D., 1967. Controlled fracture of brittle solids and interruption of electrical current. *Nature*.
[12] Silling, S. A., Demmie, P. N., & Warren, T., 2007b. Peridynamic simulation of high-rate material failure. *Sandia National Lab.(SNL-NM), Albuquerque, NM, Technical Report*.
[13] Abraham, F. F., 2001. The atomic dynamics of fracture. *Journal of the Mechanics and Physics of Solids*, vol. 49, n. 9, pp. 2095–2111.
[14] Döll, W., 1975. Investigations of the crack branching energy. *International Journal of Fracture*, vol. 11, n. Springer, pp. 184–186.
[15] Ravi-Chandar, K. & Knauss, W. G., 1984. An experimental investigation into dynamic fracture: IV. On the interaction of stress waves with propagating cracks. *International Journal of Fracture*, vol. 26, n. 3, pp. 189–200.
[16] Ramulu, M. & Kobayashi, A. S., 1985. Mechanics of crack curving and branching - a dynamic fracture analysis. In *Dynamic fracture*, pp. 61–75. Springer.